PROCEEDINGS OF SCIENCE

Production of Quarkonia States at the LHC with the ATLAS Experiment

James Walder*
On behalf of the ATLAS Collaboration
Lancaster University
E-mail: jwalder@cern.ch

Predictions for the production of quarkonia states at hadron colliders have been addressed using a number of theoretical approaches, which can now be compared to measurements performed at the LHC. In this paper, we discuss comparisons with ATLAS data taken in 2010 and 2011. In the Charmonium family, J/ψ production has been measured over a wide range of transverse momentum. In the Bottomonium family, the production of the $\Upsilon(1S)$ has been studied. The recent observation of a new particle decaying to $\Upsilon(1S)\gamma$ and $\Upsilon(2S)\gamma$, with mass about 30 MeV below the open-beauty threshold is presented. The signal is consistent with the multiplet of $\chi_b(3P)$ states predicted by potential models.

36th International Conference on High Energy Physics
4-11 July 2012
Melbourne, Australia

*Speaker.

PoS(ICHEP2012)287

1. Introduction

Theories of the production mechanisms of the bound quark-antiquark states, such as the Charmonium and Bottomonium systems, continue to be challenged by measurements in e^+e^-, hadron and heavy-ion collisions. Data from the LHC provides tests of current predictions at a new energy, and will provide important input into the further understanding and improvements of such models. Presented here are results from the ATLAS experiment using data collected in 2010 and 2011 from proton-proton collisions at $\sqrt{s} = 7$ TeV. In the Charmonium family, the production of J/ψ has been studied over a wide range of p_T, and the $\chi_c(1P)$ has been observed. In the Bottomonium family, the production of $\Upsilon(1S)$ has been studied. The observation of a new particle decaying to $\Upsilon(1S)\gamma$ and $\Upsilon(2S)\gamma$ is presented. This signal is consistent with the multiplet of $\chi_b(3P)$ states predicted by potential models [1, 2]. The ATLAS detector is presented in detail elsewhere [3]. Muons are identified and measured using the Inner Detector (ID) and Muon Spectrometer (MS). The measurement of photons is performed using either the ID or energy deposits in the Electromagnetic Calorimeter.

2. Prompt, non-prompt and inclusive measurements of the J/ψ production cross-sections

A differential inclusive, prompt and non-prompt cross-section measurement in bins of p_T and rapidity has been performed [4] using data collected in 2010 with low-p_T single-muon triggers, corresponding to a data sample of approximately 2.3 pb^{-1}, which is used to reconstruct J/ψ candidates in the di-muon decay mode. In order to correct for trigger turn-on, reconstruction efficiencies and the acceptance correction that accounts for muons traversing outside of the detector's fiducial region, a weight is applied for each candidate, and the corrected *true* yield of J/ψ signal is extracted from a fit to the weighted invariant di-muon mass distribution in each bin of p_T and rapidity. As the spin-alignment of the J/ψ is unknown under LHC conditions, and since it affects the acceptance correction term, a number of spin-alignment hypotheses are tried. The resultant envelope around the central assumption of zero polarisation is considered as an additional source of uncertainty. Figure 1(a) shows the inclusive J/ψ cross-section as a function of p_T for the central rapidity region. Good agreement is seen between LHC experiments.

Contributions to J/ψ production appear in the form of prompt production — from direct production, or through feed-down processes of higher mass Charmonium states — or, non-prompt — through the decays of B-hadrons. These processes can be distinguished using the displacement of the point of decay to that of the primary interaction using the pseudo-proper lifetime τ, defined as $\tau = L_{xy} \cdot m(J/\psi)/p_T(J/\psi)$, where L_{xy} is the transverse displacement of the decay vertex projected onto the transverse momentum. Figure 1(b) shows the fraction of J/ψ decays from non-prompt processes as a function of p_T for the central rapidity region. Good agreement is observed with the results from CDF, which suggests little dependence on $\sqrt{s}$ for this quantity.

Combining the non-prompt fraction determination and inclusive J/ψ cross-section, both the non-prompt and prompt cross-sections can be extracted, as shown in Figs. 1(c) and 1(d) respectively. The non-prompt cross-section is in good agreement with the FONLL predictions. For the prompt cross-section, the NNLO* predictions have a similar shape as the data, but a different magnitude. The Colour Evaporation Model does not describe the shape very well.

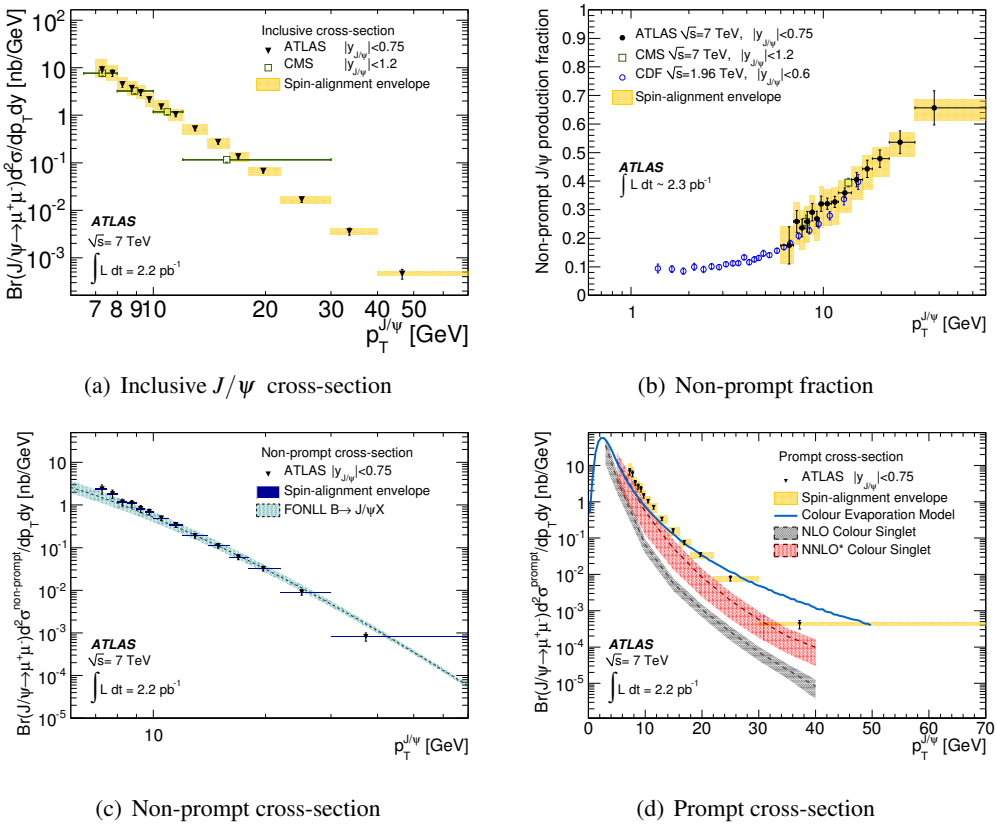

(a) Inclusive J/ψ cross-section

(b) Non-prompt fraction

(c) Non-prompt cross-section

(d) Prompt cross-section

Figure 1: The inclusive cross-section is shown in (a), non-prompt fraction in (b), the non-prompt cross-section in (c) and the prompt cross-section is shown in (d). All cross-sections are shown as a function of p_T for the rapidity region $|y(J/\psi)| < 0.75$ with comparisons to various experimental results and theoretical predictions. Additional rapidity regions $0.75 < |y| < 1.5$ and $1.5 < |y| < 2.0$ have also been measured [4].

3. Measurement of the $\Upsilon(1S)$ fiducial cross-section

The cross-section measurement of the $\Upsilon(1S)$ state has been performed [5] as a function of p_T for two regions of rapidity, using the decay mode $\Upsilon(1S) \to \mu^+\mu^-$ in the fiducial region defined by $p_T(\mu) > 4$ GeV and $|\eta(\mu)| < 2.5$, using data collected in 2010, corresponding to $\mathscr{L} = 1.13$ pb^{-1}. As in the case of the J/ψ , each candidate receives a weight to account for inefficiencies in the trigger and muon reconstruction.

Using template based methods, the corrected yields in each p_T and rapidity bin are extracted, and the resultant differential cross-sections are shown in Fig. 2. The NRQCD prediction is similar in magnitude to the data, although the shape is not well described. The Colour Singlet Model using NLO predictions is low compared to the data; although, it does not contain feed-down from the higher order states. As the events are not corrected for acceptance, this measurement is therefore independent of any assumptions as to the spin-alignment and can therefore precisely test theoretical predictions.

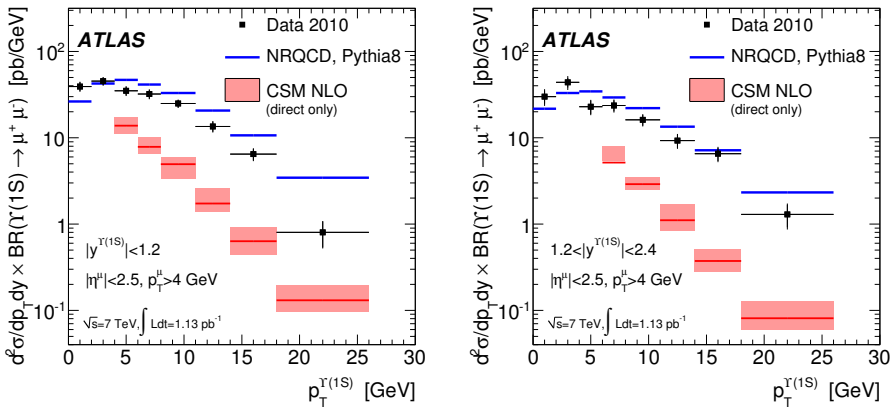

(a) (b)

Figure 2: The differential fiducial cross-section of the $\Upsilon(1S)$ measured through the decays into two muons is shown as a function of p_T for the central (a) and forward (b) rapidity regions [5].

4. Observation of χ_{c1}(1P) and χ_{c2}(1P) Charmonium states

The contribution to the S-wave Charmonium (Bottomonium) states through the feed-down of the higher P-wave χ_c (χ_b) states is thought to be considerable, and hence a measurement of these states and their feed-down processes is important in understanding quarkonium production processes. The $\chi_c(1P)$ $(J = 1,2)$ states are observed [6] through radiative decays to J/ψ $(\to \mu^+\mu^-)$ using data collected in 2010, corresponding to $\mathscr{L} = 39$ pb^{-1}. The events are required to pass a low-p_T single muon trigger.

To reconstruct χ_c candidates, a J/ψ $(\to \mu^+\mu^-)$ candidate $(p_T(\mu) > 2.5$ GeV) is combined with a photon with $E_{\mathrm{T}} > 2.5$ GeV, as identified using the electromagnetic calorimeter. Candidates are retained if $p_T(\chi_c) > 10$ GeV and $|y(\chi_c)| < 2.4$ and the cosine of the opening angle between the J/ψ and the photon momenta is greater than 0.99. To effectively remove the di-muon resolution the invariant mass-difference $\delta m = m(\mu\mu\gamma) - m(\mu\mu)$ is constructed.

A simultaneous fit is performed to a signal region, defined using events with a mass-window around the J/ψ , and background, defined by events within the J/ψ sideband region. The background component of the data is used to constrain the shape of the background under the signal peak. The mass difference between the χ_{c1} and χ_{c2} is fixed to the known value and an extended unbinned maximum likelihood fit is performed. Figure 3 shows the data for the signal and sideband data distributions overlaid with the result of the simultaneous fit. From the fit, $2960 \pm 160\,(\mathrm{stat.}) \pm 120\,(\mathrm{syst.})$ χ_c events are observed, where the dominant contribution to the systematic uncertainty is from the modelling of the shape of the background.

5. Observation of $\chi_b(1P)$, $\chi_b(2P)$ and first observation of a new Bottomonium state

The $\chi_b(1P)$ and $\chi_b(2P)$ states are observed [7] through their radiative decays to $\Upsilon(1S)$ using data collected in 2011, corresponding to $\mathscr{L} = 4.4$ fb^{-1}, using a suite of single and di-muon triggers. Two oppositely-charged muons with $p_T(\mu) > 4$ GeV, $|\eta(\mu)| < 2.3$ are combined to form the Υ

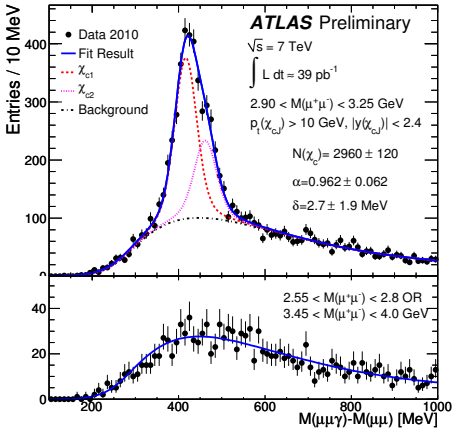

Figure 3: The invariant mass-difference $\delta m = m(\mu\mu\gamma) - m(\mu\mu)$ of χ_c is plotted for the result of the simultaneous fit to signal candidates (top) within the J/ψ mass-window and background from the J/ψ sidebands. Overlaid on the data are the projections of the result of the fit [6].

candidate. In addition to the $\chi_b(1P)$ and $\chi_b(2P)$ states, the first observation of a higher mass state, compatible with $\chi_b(3P)$ is observed in transitions to both $\Upsilon(1S)$ and $\Upsilon(2S)$.

Photons can either be reconstructed through identification of energy deposits in the electromagnetic calorimeter, a sample referred to as Unconverted, or if the photon converts within the tracking volume of the detector, it can be identified by reconstructing two tracks in the ID originating from a common vertex, and with the radial distance from the beam-line of at least 40 mm. This sample is referred to as Converted. Unconverted photons have a reconstruction threshold of $E_T > 2.5$ GeV, whereas for Converted photons each track must have $p_T(e) > 0.5$ GeV and $p_T(\gamma) > 1$ GeV. The photons are required to be consistent with having originated from the di-muon vertex. As stated previously, the mass difference $\delta m = m(\mu\mu\gamma) - m(\mu\mu)$ is used to minimise the effects of detector resolution.

Figure 4(a) shows the mass distribution for χ_b candidates decaying to $\Upsilon(1S)\gamma$ candidates, where the photons are from the Unconverted sample. The data shows the $\chi_b(1P)$ and $\chi_b(2P)$ peaks and shows an additional peak. From the unbinned likelihood fit to the data, the mass of the third peak is estimated to be $m = 10.541 \pm 0.011\,(\text{stat.}) \pm 0.030\,(\text{syst.})$ GeV. Figure 4(b) shows the mass distribution for χ_b candidates decaying to $\Upsilon(1S)\gamma$ candidates, where the photons are from the Converted sample. Overlaid is the result of the simultaneous fit to the two mass distributions. The $\chi_b(1P) \to \Upsilon(1S)\gamma$ and $\chi_b(2P) \to \Upsilon(1S)\gamma$ peaks are both visible. An additional peak is observed through transitions to both the $\Upsilon(1S)$ and $\Upsilon(2S)$. The difference in the observed peak positions is due to the different magnitudes of the energy loss effects on the converted photon for each transition. From the fit, where the mass of the $\chi_b(1P)$ and $\chi_b(2P)$ peaks are constrained to their known values, the mass of the additional peak is measured to be $m = 10.530 \pm 0.005\,(\text{stat.}) \pm 0.009\,(\text{syst.})$ GeV. As the mass difference between the hyperfine states corresponding to $J = 1, J = 2$ is similar to the detector resolution, and the $J = 0$ contribution is heavily suppressed in radiative decays, an equal contribution of $J = 1, J = 2$ is assumed for each peak. This assumption is varied in order to determine the relevant contribution to the systematic uncertainty.

This third peak, observed using converted and unconverted photons through radiative decays

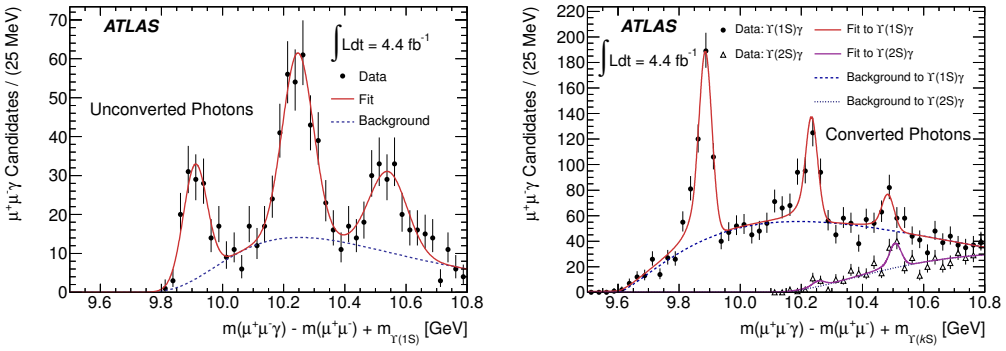

(a) Unconverted (b) Converted

Figure 4: The mass distributions of $\chi_b \to \Upsilon(1S)\gamma$ candidates for unconverted photons (a) reconstructed from energy deposits in the electromagnetic calorimeter, and $\chi_b \to \Upsilon(kS)\gamma$ ($k = 1,2$) candidates formed using photons which have converted (b) and been reconstructed in the ID. Data are shown before the correction for the energy loss from the photon conversion electrons due to bremsstrahlung and other processes. The data for decays of $\chi_b \to \Upsilon(1S)\gamma$ and $\chi_b \to \Upsilon(2S)\gamma$ are plotted using circles and triangles respectively. Solid lines represent the total fit result for each mass window. The dashed lines represent the background components only [7].

to $\Upsilon(1S)$ and $\Upsilon(2S)$ is interpreted as deriving from the $\chi_b(3P)$ system. This new state now implies that all of the $\Upsilon(1S)$,$\Upsilon(2S)$ and $\Upsilon(3S)$ (although not directly observed) states receive contributions from feed-down of higher mass states. Therefore it is the $\psi(2S)$ that remains the only quarkonium state unaffected from feed-down from higher mass states.

6. Conclusions

Using data collected by the ATLAS Experiment in 2010 and 2011 in proton-proton collisions at $\sqrt{s} = 7$ TeVat the LHC, Charmonium and Bottomonium states have been observed, including a new state interpreted as $\chi_b(3P)$. Measurements of their production mechanisms have also been performed. With these and future measurements of the heavy quark–antiquark bounds states, further insights into the nature of Quantum Chromodynamics close to the strong decay threshold will emerge.

References

[1] W. Kwong and J. L. Rosner, Phys. Rev. D **38** (1988) 279.

[2] L. Motyka and K. Zalewski, Eur. Phys. J. C **4** (1998) 107

[3] ATLAS Collaboration, JINST **3** (2008) S08003.

[4] ATLAS Collaboration, Nucl. Phys. B **850** (2011) 387 [arXiv:1104.3038 [hep-ex]].

[5] ATLAS Collaboration, Phys. Lett. B **705** (2011) 9 [arXiv:1106.5325 [hep-ex]].

[6] ATLAS Collaboration, ATLAS-CONF-2011-136

[7] ATLAS Collaboration, Phys. Rev. Lett. **108** (2012) 152001 [arXiv:1112.5154 [hep-ex]].